International Journal of Thermal Sciences 190 (2023) 108292

Contents lists available at ScienceDirect

International Journal of Thermal Sciences

journal homepage: www.elsevier.com/locate/ijts

Direct absorption solar collector: Use of nanofluids and biodegradable colloids

Linna V. Nguyen [a], Pawel Kosinski [a], Boris V. Balakin [b], Anna Kosinska [b,*]

[a] Department of Physics and Technology, University of Bergen, Norway
[b] Western Norway University of Applied Sciences, Department of Mechanical and Marine Engineering, Norway

ARTICLE INFO

Keywords:
Nanofluids
Solar energy
Solar thermal technology
Coffee colloids
Carbon black

ABSTRACT

In this paper, an experimental and numerical analysis was performed on both carbon black nanofluids and a biodegradable fluid in a novel pump-free direct absorption solar collector (DASC). In the experiments, the nanofluid consisted of carbon black nanoparticles in water with concentrations ranging from 0.005 to 0.020 wt%, while the biodegradable fluid was coffee colloid. The overall findings indicated a concurrence: the nanofluids exhibited the best thermal performance when compared to pure water. The optimum nanoparticle concentration of 0.010 wt% carbon black yielded a 102% thermal enhancement compared to the base fluid. Furthermore, a numerical analysis using computational fluid dynamics (CFD) software was performed to study the experimental rig. According to these simulations, the optimal nanofluid concentration showed a 76.6 - 90.9% increase compared to the base fluid. The biodegradable fluids did not show a significant enhancement in the experiments, which differs from what has been reported in the scientific literature. Nevertheless, from the computer simulations, the biodegradable fluids also slightly outperformed the case when the pure water was used.

1. Introduction

With the growing global demand for energy and the challenges associated with power generation, there is a need for continuous, sustainable access to energy sources. One solution is solar energy, which has the potential to provide unlimited access to renewable resources.

An interesting approach is the use of direct absorption solar collectors (DASCs), which are based on the principle of absorbing incident solar radiation by the volume of the working fluid in the system [1]. The use of DASCs eliminates layers of tubes and absorber plates seen in conventional solar thermal technology, resulting in lower thermal resistance to solar thermal energy conversion. Moreover, the volumetric absorption reduces the exterior absorber temperature, and thereby the thermal losses [2,3]. Ultimately, higher system efficiency is achieved for the DASCs, as researchers have reported a 5%–20% efficiency increment when comparing nanofluid-based DASCs with conventional surface-based solar collectors [3–12]. It is interesting to note that a similar issue exists in the field of photonics, where there is a need for the development of solar absorbers, see e.g. [13–15].

Over the past decades, researchers have made many attempts to improve the efficiency of solar collectors. Conventional heat transfer fluids such as water, oil, and ethylene glycol may enhance their thermal efficiency at high flow rates, but this also increases pumping costs and reduces overall efficiency. One promising solution is the use of working fluids with better heat transfer characteristics. Studies have shown that using nanofluids in solar systems offers distinct benefits over conventional fluids.

Since the phenomenon of nanofluids was proposed by Choi and Eastman [16], there has been tremendous growth in their use in various applications [9,17–19]. Nanofluids, which comprise stable suspended nanosized particles in a base fluid such as water, have significantly increased conductive and convective heat transfer properties. Their use in solar energy can improve thermal and optical properties, leading to their wider use in solar thermal technology [18–23].

Despite the effective ways that nanofluids can increase heat generation through radiation, there are some concerns associated with their usage, including high production costs, clogging, and nanotoxicity [24]. This has limited the practical application of nanofluids, leading to the exploration of alternative fluid compositions [25–28]. A growing trend in recent research is the use of bio-based materials as alternatives to minimise the use of hazardous components. For example, coffee-based suspensions have been proposed as an inexpensive, stable, and biodegradable alternative for solar thermal applications [25–27,24]. Further analysis is required to evaluate the potential positive impact that these biodegradable fluids could have in energy solutions.

* Corresponding author.
E-mail address: anna.dorota.kosinska@hvl.no (A. Kosinska).

https://doi.org/10.1016/j.ijthermalsci.2023.108292
Received 24 January 2023; Received in revised form 18 February 2023; Accepted 16 March 2023
Available online 27 March 2023

The main aim of this research was to study the thermal performance of different working fluids in solar thermal energy applications. In this study, three types of fluids were experimentally and numerically tested in a direct absorption solar collector (DASC) experimental set-up: water, biodegradable fluids, and nanofluids. The research also examined a range of low particle concentrations for nanofluids in order to identify the optimal concentration with strong heat absorption capabilities. In addition, a numerical approach was used to provide further insights into the system.

What distinguishes this paper from similar works is its utilisation of a pump-free system. Although a pump can ensure a constant flow of the working fluid into the system, it can also increase the fluid temperature and potentially cause heat generation during operation. This is particularly critical in laboratory-scale applications that have low heat transfer rates but high pumping expenses, as pump-generated heat can be substantial in small flow channels. Therefore, the objective of this paper was to focus solely on the volumetric heat generation of the experimental setup.

Furthermore, biodegradable colloids and nanofluids were previously compared in our two recent papers [27,29]. However, the focus in those papers was on stationary fluids and their optical properties, and not on their use in direct absorption solar collectors. Therefore, we address this issue in the present paper.

Finally, biodegradable colloids have been studied in direct absorption solar collectors by [25]. However, our flow rates (as shown later) are one order of magnitude greater than in that work. This makes it important to investigate whether the increase in flow velocity leads to similar conclusions.

2. Experimental set-up

The laboratory set-up depicted in Fig. 1 includes a pipe system consisting of transparent glass tubes (D_{inner} = 4 mm, D_{outer} = 6 mm) connected with elbows. The design being studied also consisted of two halogen lamps (400 W/230 V) simulating solar radiation, which were directed towards a pipe system containing a given working fluid. The pipe system was located at a distance H = 10.5 cm away from the lamps. As a result, our rig differed from the more common flat-plate or u-tube solar collectors.

The working fluid was initially placed in the inlet beaker so that the flow was due to gravity. Hence, as indicated in the previous section, no pump to transport the fluid was used in the system.

The length of the irradiated pipe was 0.72 m, while the overall total length of the pipe system was 3.0 m. Two K-type thermocouples for temperature measurements were attached to the inlet and outlet of the experimental set-up. The inlet and outlet were located behind cardboard partitions to prevent heat transfer by radiation to the thermocouples and working fluid. For each experiment, temperature data was recorded by a Multilogger Thermometer (HH506RA) from Omega Engineering.

Various methods exist to mimic solar radiation, and in this experimental rig, two halogen lamps were utilised for this purpose as already mentioned. However, it must be stated that use of the lamps did not exactly match the solar spectrum in practical applications but yielded a controlled environment for repeated experimentation. Additionally, a solar power meter (LS122 IR, Linshang Technology) was applied to map the radiation intensity at the top surface of the experimental set-up. The resulting radiation map is displayed in Fig. 2. The estimated average heat flux over the irradiated area of the system was approximately 5000 W/m^2 (equivalent to 5 suns). This value was also used in our computer simulations described later in the paper.

The preparation of nanofluids followed the two-step method, which appears to be commonly exploited in the literature [6,27,29–33]. The carbon black nanoparticles ENSACO™ 350G from Timcal with a bulk density of 2250 kg/m^3 were used to synthesise nanofluids [33]. In addition, the surfactant sodium dodecyl sulphate (SDS) with a bulk density of 1010 kg/m^3 was added to ensure stability for the nanofluids [34].

To synthesise the nanofluids, a similar method to [27,35] was implemented. Depending on the required concentration of nanoparticles in the nanofluid, a specified amount of carbon black nanoparticles was weighed (precision scale from Sartorius) and mixed with the equal amount of SDS in the base fluid, distilled water. We thereby followed the same procedure as in the works by Kosinska et al. [27] and Otanicar et al. [31], who used the same mass of SDS as nanoparticles in their preparations. The weight measurements had an accuracy of ± 1 mg using an analytical scale.

A magnetic stirrer (VWR VMS-C4 Advanced, 1500 rpm) was then used to mix the suspension of distilled water, nanoparticles and SDS for 20 min. Next, a second step followed, placing the beaker in an ultrasonic bath (Branson 3510, 130 W) with an ultrasonication level of 40 kHz. The purpose of using ultrasonic waves was to homogenise the nanofluids by breaking the agglomerates [35,19]. The suspension was sonicated for one hour. The manufactured nanofluids were stable (naked-eye observations) for at least a few months.

Five different weight concentrations of carbon black nanoparticles were produced, namely 0.005 wt%, 0.010 wt%, 0.015 wt%, 0.020 wt% and 0.050 wt%, differing from other papers that consider much higher concentrations [27,29].

Kosinska et al. [27] reported that coffee samples of weight 15.0 g dissolved in 300 ml distilled water show satisfactory results. In our work, the proportion of tap water for the fluid preparations was equivalent to the distilled water used in [27]. Thus, this study's ideal concentration in biodegradable fluids was set at 0.05 g coffee colloid (CC) per 1 ml, close to what the other researchers applied.

A coffee brewer from Russell Hobbs (Elegance 23370-56) was used for the preparation of the biodegradable fluid. In the process, we initially used cold and fresh tap water (with a temperature of 6 °C) with filter ground coffee (arabica and robusta) from Friele. The resulting fluid was then cooled prior to experimentation.

In the experiments, tap water and distilled water were used and form the basis for comparison as water has versatile usability, including being used in conventional solar absorption applications. While the tap water was provided in March 2022 from the Bergen (Norway) drinking water supply, the distilled water was from Fybikon AS.

Firstly, the required working fluid was synthesised using the above preparation methods. The fluid volume of 3 L was selected. Next, in the experimental part of this study, our main objective was to estimate the fluid flow in the pipe system, the extinction coefficient corresponding to each working fluid, and the resulting radiation at the pipe system surface. Lastly, our findings were compared with numerical analysis.

The following procedure was followed for all the working fluids. A given fluid was placed in the inlet beaker at a set fluid level to ensure a repetitive procedure. The fluid had an initial temperature equivalent to the ambient temperature prior to each experiment. Here, the temperature difference between the temperature of the set-up and surroundings were not allowed to exceed ±0.3 °C.

The fluid level was regulated manually by adjusting its height to a range between 0.86 to 0.96 meters. The volumetric flow rate at the outlet was estimated by logging it using a graduated cylinder with a capacity of 250 ml and by recording the time interval between each 10 ml. The fluid flow measurements were repeated for each working fluid included in the experiment and yielded an average fluid velocity of 0.398 ± 0.056 metres per second for all the working fluids. The average flow rate was thus 5 ml/s. The experiments were repeated at least five times for each working fluid after resetting the experimental set-up and ensuring that it reached the same temperature as the ambient air between each repetition.

3. Results: photo-thermal experiments

The following section presents the experimental results for the system and working fluids studied, including water as the base fluid, together with four concentrations of carbon black nanofluids with

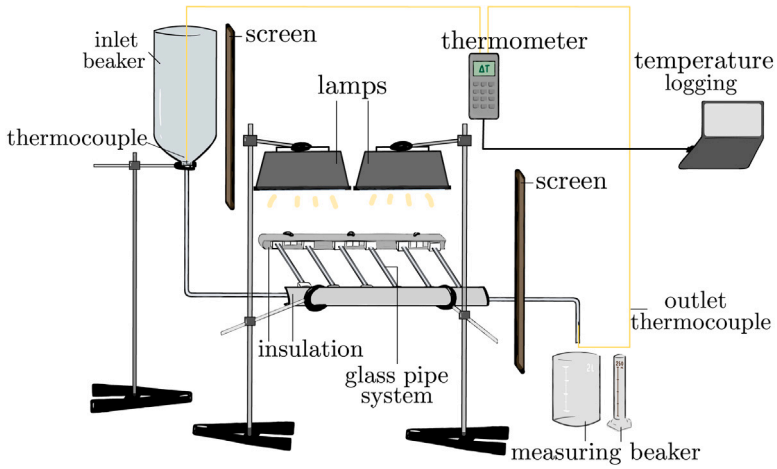

Fig. 1. Schematic of the experimental set-up (not to scale). The included pipe system is oriented horizontally beneath and parallel to two halogen lamps, while the container with the various working fluids is positioned perpendicular to the pipe system.

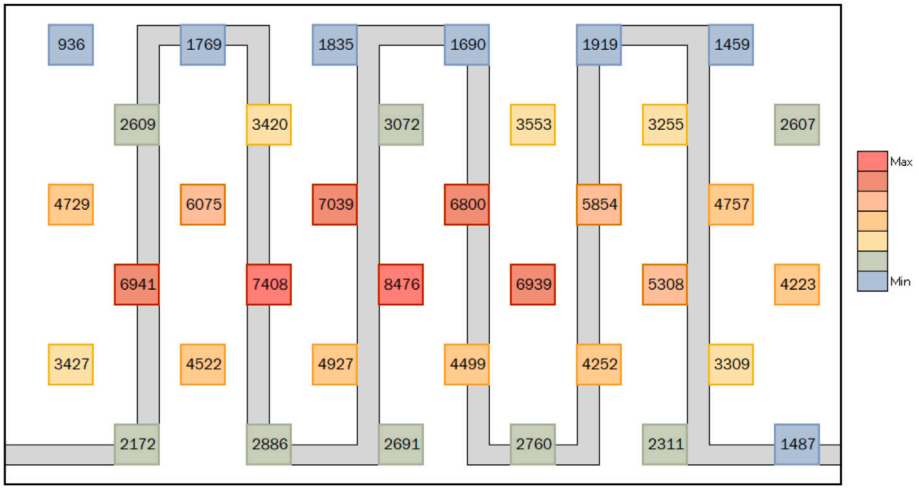

Fig. 2. Radiation map of the pipe system (depicted in grey), located at distance H = 10.5 cm away from the radiation source. The light intensity was measured in W/m^2.

SDS and one concentration of a biodegradable fluid. The fluids were prepared and examined in the experimental set-up as described in the previous section. All the experimental studies used initially cooled halogen lamps at room temperatures ranging from 21 to 25 °C. Fig. 3 gives an overview of the results obtained from the photothermal experiments for the working fluids in the study. The figure shows the increase in fluid temperature as it flows through the pipeline during irradiation.

Furthermore, for illustration, Fig. 4 shows the temperature history for distilled water in five different experiments. Similar behaviour was also observed for the other fluids. In all the cases studied, a rapid increase in temperature occurs at the start of the process, followed by stabilisation. Additionally, the temperature tends to rise gradually due to the unavoidable heating of the experimental set-up and the surrounding air.

As the experiments involved several concentrations of nanofluids, their performance in a DASC is therefore discussed. When using carbon black nanofluids as the working fluid, the highest mean temperature difference achieved was 1.74 °C, as indicated in Fig. 3. This corresponded to a nanofluid concentration of 0.010 wt%.

While the use of carbon black nanoparticles resulted in greater absorption compared to conventional fluids, it is important to consider the effect of volume fraction on the optical properties of the fluid. Experimental results reported by [36,37] demonstrate enhanced thermal performance at an optimum nanoparticle concentration of 0.010 wt%. This is in line with our findings.

As discussed by many other researchers, the enhanced heat absorption abilities of nanofluids are mainly due to the increased surface area provided by the nanoparticles. Thus, as more nanoparticles absorb the incoming radiation, there is an increase in heat generation in the fluid. Nevertheless, as the number of particles continues to increase beyond a certain value, the radiation is only absorbed by the nanoparticles near the surface, which intensifies the heat loss to the surroundings and reduces the system's overall heat absorption.

The thermal performance of a nanofluid-based DASC was also investigated through numerical and experimental studies conducted by [38,31]. These studies found the collector performance to be highly dependent on the concentration of nanoparticles. Additionally, efficiency was also found to improve with increasing fluid depth. Crega and Myers [38] also observed a limit beyond which adding more particles becomes ineffective. Efficiency increases rapidly for small volume fractions, but after a certain point, the rate of increase in efficiency begins to decrease [31]. Problems such as aggregation, sedimentation, and higher viscosity that come with higher nanoparticle concentrations may be contributing factors to this.

According to the studies presented above, all the nanoparticle concentrations considered outperformed the water and biodegradable fluids, with a 67%–102% thermal enhancement from the base fluid. The biodegradable fluids resulted in performance similar to that of water. It is worth noting that Kosinska et al. [29] reported that a biodegradable fluid with coffee colloids had the best temperature rise when compared

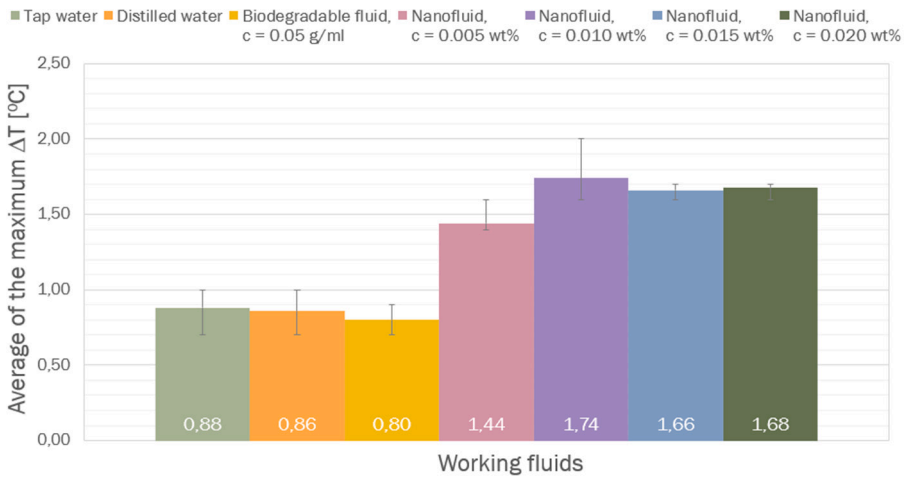

Fig. 3. The average temperature difference obtained from the experiments for all the working fluids. The bars indicate the range of temperature differences observed in the experiments.

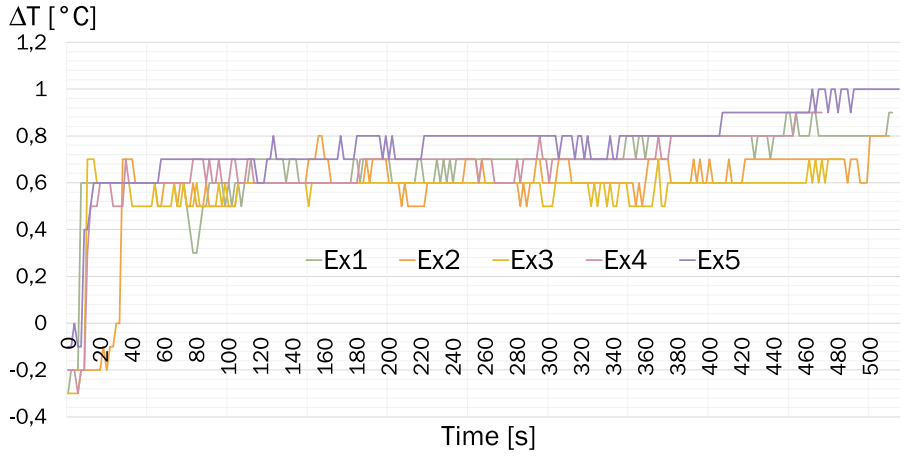

Fig. 4. The temperature difference for distilled water, ΔT [°C], between the inlet and outlet temperatures as a function of time [s]. The five experiments conducted are labelled from Ex1 to Ex5.

to distilled water and nanofluids with particle concentrations between 0.25% and 1.00%. However, this is not evident from this study, when much smaller nanoparticle concentrations were examined. Furthermore, Kosinska et al. [29] found a thermal efficiency enhancement of 2% when carbon black nanofluids were compared with the highest concentration of coffee colloids equivalent to the concentration studied here.

Nevertheless, the biodegradable fluid did not outperform the base fluid in our research. This is in contrast to other studies, which report improved heat absorption for applications using coffee-based colloids compared to pure water [27,29,26]. However, the aforementioned studies included stationary fluids subject to radiation [27,29], solar-based desalination systems [26], or a system with a significantly lower flow rate than the one studied by us [25]. Therefore, none of the systems are similar to our experimental set-up. The higher temperature increase found in the literature is expected, as lower flow rates would provide more heating generated for the system, resulting in better heat absorption for the working fluid.

Some uncertainties that arose during experimentation concerned whether the working fluid was directly heated up by the lamps or also by the glass tubes (that were essentially heated up by the lamps). These effects may also have dominated the results so that the enhanced properties of the biodegradable fluids were not sufficient to give better performance than the base fluid.

4. Computer simulations

In addition to the experiments, we conducted simulations using Computational Fluid Dynamics (CFD) software, Simcenter STAR-CCM+. The fluid flow was chosen to be laminar, due to the low velocity, and the fluid was not affected by radiational heat. In other words, the objective of this simulation stage was primarily to analyse the flow in the main system. The software solved the standard Navier–Stokes equations for an incompressible flow with an energy equation. Since the concentration of nanoparticles and coffee colloids suspended in the working fluids was low, no additional modifications to the fluid properties took place. As a result, the thermal properties of the various working fluids were equivalent to those of water.

Later, as the fluid flow became steady, a volumetric heat generation was included in the model. For this, we assumed that the radiation was one-dimensional (in the direction perpendicular to the pipeline system). The maximum radiation intensity, I_o [power/area], occurred at the surface where $x = 0$. The Beer–Lambert law describes decaying radiation intensity associated with the propagation length, x, within the fluid as (see e.g. our previous work [29] for a similar model):

$$I = I_0 \exp[-Kx], \tag{1}$$

where K denotes the extinction coefficient (discussed below).

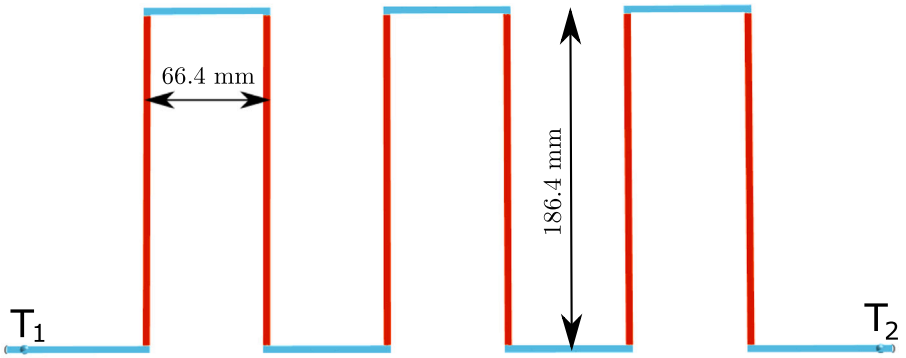

Fig. 5. Snapshot of the main system with the average volumetric heat absorption generated in STAR-CCM+. The blue region indicates no heat generation, while the red indicates areas with volumetric heat absorption. The temperature was monitored in points T_1 and T_2.

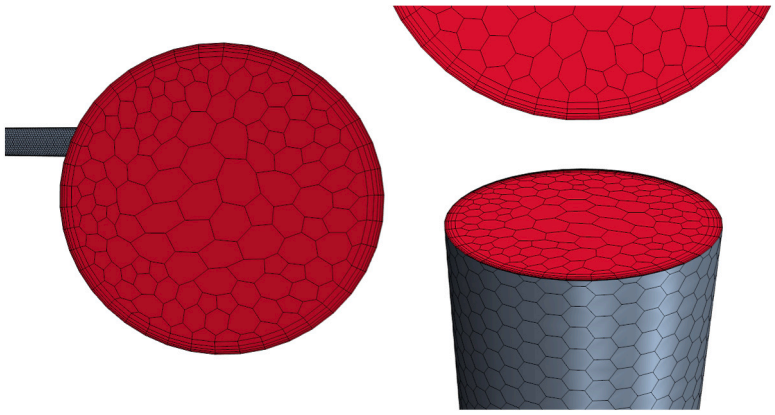

Fig. 6. Computational mesh used in the simulations.

The volumetric heat generation, q_v, [power/volume] can furthermore be calculated:

$$q_v = -\frac{\mathrm{d}I}{\mathrm{d}x} = I_0 K \exp\left[-Kx\right]. \tag{2}$$

From this, we computed the total heat generation by estimating the mean of the above function, which was later implemented as a source term in the aforementioned energy equation solved by the computational software:

$$\overline{q_v} = \frac{1}{s}\int_0^s q_v(x)\mathrm{d}x = \frac{I_o}{s}[1-\exp(-Ks)], \tag{3}$$

where s is the characteristic thickness of the system. In this research, the characteristic thickness was found as shown below.

The glass tubes that are subject to radiation are cylindrically shaped, with an internal diameter, D_i. For simplicity, we stated that the cross-sectional area of the cylindrical tubes is equal to the cross-sectional area of a square with size s. It can also be assumed that the irradiation is distributed uniformly in this cross-section. By considering the cross-sectional areas to be equal, the geometric dimension of the square, s, can be estimated by equating: $\pi D_i^2/4 = s^2$. Therefore: $s = \sqrt{\pi} D_i/2$.

The walls that make up the pipe system were chosen to be adiabatic, meaning that no heat flux is permitted to pass through, except for the transmitted radiation from the lamps. In this study, the Boussinesq model was applied, which includes a buoyancy source term in the Navier–Stokes equations. This model assumes only small changes in density due to temperature variations.

The boundary condition associated with the inlet was set to a constant static temperature of 20 °C (293.15 K) and a constant velocity magnitude corresponding to the fluid flow velocity obtained from initial experimentation (0.398 m/s, as noted in Section 2). The walls were all set to be no-slip.

Fig. 5 shows the computational domain. The volumetric heat absorption was only taken into account in the areas of the experimental set-up exposed to radiation. In the simulations conducted, the heat was absorbed in the red regions. No radiation reached the parts of the system shown in blue, as they were insulated in the experiments. Additionally, it was assumed that no heat was transferred to the fluid before and after the turns in the pipeline. The radiation intensity, I_0, at the top of the system was set to 5000 W/m^2 (equivalent to 5 suns). This was approximately consistent with the experimental observations, although the actual irradiation distribution was not uniform, as discussed earlier. The temperature difference in the system was calculated by monitoring the temperatures close to the inlet and outlet.

The computational mesh is depicted in Fig. 6. The mesh consists of polyhedral cells and five prism layers close to the wall. This was selected after a series of grid dependency studies.

Before the simulations, the extinction coefficient was measured experimentally using a simple set-up. For this purpose, a sample fluid was placed in a beaker, and the light from the lamp was passed through it. The distance from the lamp was 10.5 cm, which was the same as in the other experiments. The light intensity was measured using the previously mentioned solar power meter. This approach took advantage of the simplicity of Beer–Lambert's law, while also accounting for the extinction coefficient for the set-up used in this research.

For various carbon black nanoparticle concentrations, the extinction coefficient measured, together with results found in the literature are given in Fig. 7. The figure shows our results for two cases: (i) averaged values obtained for different fluid thicknesses; (ii) the thickness of the fluid was 5 mm, which also corresponded to the size of the pipes used in our experimental rig. We note that there is almost no difference between these two cases, as the extinction coefficient was not dependent on the fluid's thickness.

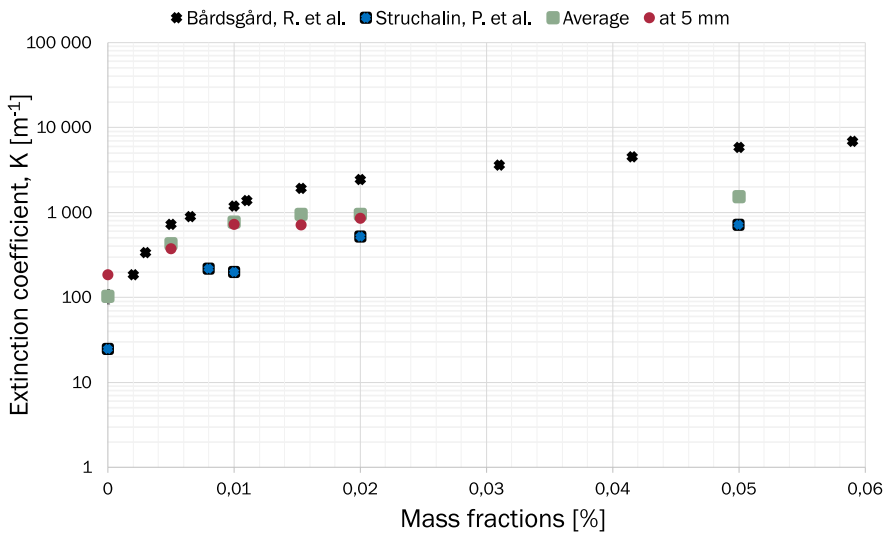

Fig. 7. Estimations of the extinction coefficient for different mass fractions of carbon black nanofluids for two cases: (i) averaged values obtained for different fluid thicknesses, (ii) the thickness of the fluid was 5 mm. The results are compared to literature values from Bardsgard et al. [39] and Struchalin et al. [37].

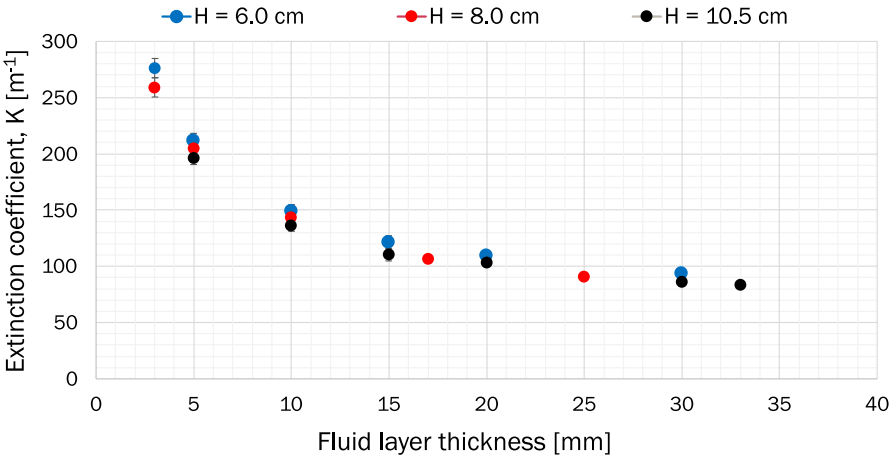

Fig. 8. Estimations of the extinction coefficient for biodegradable fluids at alternating height distances from the lamp, H = 6.0 cm, 8.0 cm and 10.5 cm. The error bars indicate the standard deviation of the data at different fluid thicknesses.

The values provided in the literature by Bardsgard et al. [39] and Struchalin et al. [37] differ from the compositions of nanofluids studied in the present work. Bardsgard et al. also studied carbon black nanofluids, but their extinction coefficients were calculated theoretically, whereas Struchalin et al. experimentally determined the extinction coefficient for carbon nanotube-based nanofluids.

For biodegradable fluids and water, the extinction coefficient decreases as the fluid layer thickness increases, due to Rayleigh scattering. This trend is illustrated in Fig. 8 for a coffee colloid (a similar trend was observed for water).

For our computer simulations, we selected the following values of the extinction coefficient: (i) water 186.6 m^{-1}, (ii) biodegradable fluid: 196.7 m^{-1}; and (iii) nanofluid (0.01%): 730.5 m^{-1}. These values were obtained for the fluid depth of 5 mm, which directly corresponded to the pipe size used in our experiments. Thus, they were not the same as used by the other researchers.

5. Simulation results

It is important to note that the actual temperature increase recorded from experiments and simulations may differ. As previously mentioned in the paper, in addition to heating the fluid through radiation absorption, the lamps also raised the temperature of the glass wall in the pipe system. This results in forced convection that enhances heat transfer to the fluid in the system under the influence of the radiating lamps. However, this effect is challenging to model correctly and was not taken into account in our simulations. Therefore, the focus of this research was on a more qualitative comparison between the fluids studied, investigating how they performed relative to each another.

The temperature increases for the three cases studied were as follows according to the simulations: (i) 0.452° for water, (ii) 0.469° for the biodegradable fluid; and (iii) 0.866° for the nanofluids. As expected, the simulated temperature increases are below the experimental values shown in Fig. 3.

Next, we present the relative temperature increase related to the base fluid (water), and these results are summarised in Fig. 9. The figure compares the simulations with the experiments, and reveals that there is a very satisfactory agreement between the experiments and the simulations.

We notice that the temperature increase for the biodegradable fluid is only 4% greater than for water. This finding is partially supported by the experimental results, which showed no significant difference. Interestingly, the extinction coefficients, for water and biodegradable fluids differ by around 5%, which is of a similar order of magnitude to the temperature increase obtained. It is also clear that the nanofluid outperformed the other fluids. Compared to water, the temperature rise

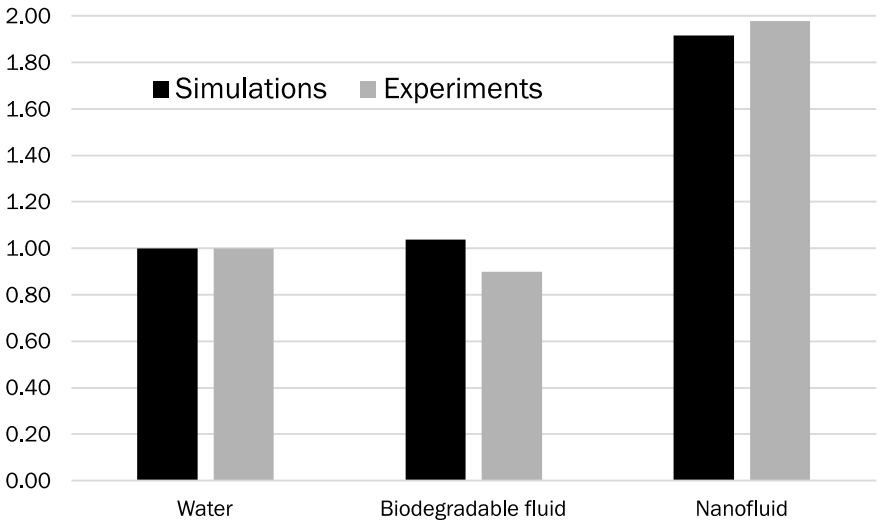

Fig. 9. Temperature increase results from the simulations for all the working fluids.

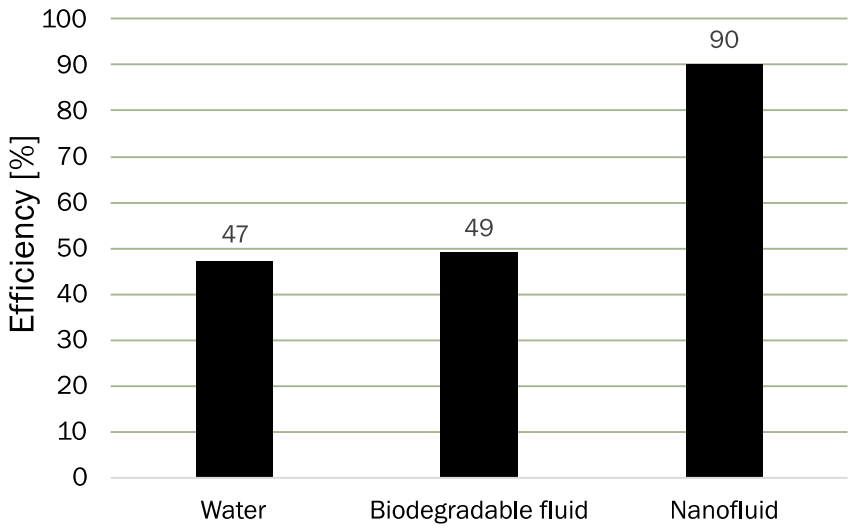

Fig. 10. Thermal efficiency of the simulated system.

is 92% greater according to the simulations. From the experiments, the corresponding rise is 97%.

Finally, we calculated the thermal efficiency by relating the thermal energy output obtained by the system to the total irradiation energy [19,31,37,40,41]:

$$\eta = \frac{\dot{m} C_p \Delta T}{I_o A}, \tag{4}$$

where $\dot{m} = 0.005$ kg/s is the mass flow rate, $C_p = 4180$ J/(kg·°C) is the heat capacity (assuming the properties of water), and $A = 0.004$ m^2 is the irradiated area. The temperature increase was the same as depicted in Fig. 9.

The results are depicted in Fig. 10, and they confirm a high thermal efficiency for the nanofluids. For a nanoparticle concentration of 0.010 wt%, such efficiencies are in agreement with the literature findings [37].

6. Concluding remarks

In this paper, experiments were conducted to gain a deeper understanding of the thermal performance of various working fluids in solar thermal applications, including water, biodegradable fluids, and nanofluids. The focus of the study was on the volumetric absorption of solar energy within the fluids, using a simple experimental set-up and two simulation models.

Although biodegradable fluids based on coffee colloids are considered a suitable replacement for nanofluids, the research confirms that nanofluids result in the best performance when used in direct absorption solar collectors.

The study also shows that modelling of the direct absorption solar collectors can be obtained by using a simple model based on Beer–Lambert's law, despite challenges related to simulating all processes such as heat absorption by the pipe walls. Nonetheless, the results are qualitatively accurate.

Declaration of competing interest

The authors declare that they have no known competing financial interests or personal relationships that could have appeared to influence the work reported in this paper.

Data availability

Data will be made available on request

Acknowledgements

The simulations were performed on resources provided by Sigma2 - the National Infrastructure for High Performance Computing and Data Storage in Norway.

References

[1] J.E. Minardi, H.N. Chuang, Performance of a "black" liquid flat-plate solar collector, Sol. Energy 17 (3) (1975) 179–183.
[2] J.R. Eggers, M. Lange, S. Kabelac, Radiation and energetic analysis of nanofluid based volumetric absorbers for concentrated solar power, Nanomaterials 8 (2018) 838.
[3] R. Saidur, T.C. Meng, Z. Said, M. Hasanuzzaman, A. Kamyar, Evaluation of the effect of nanofluid-based absorbers on direct solar collector, Int. J. Heat Mass Transfer 55 (2012) 5899–5907.
[4] S. Delfani, M. Karami, M.A.A. Bahabadi, Experimental investigation on performance comparison of nanofluid-based direct absorption and flat plate solar collectors, Int. J. Nano Dimens. 7 (2016) 85–96.
[5] S. Parvin, R. Nasrin, M.A. Alim, Heat transfer and entropy generation through nanofluid filled direct absorption solar collector, Int. J. Heat Mass Transfer 71 (2014) 386–395.
[6] P. Raj, S. Subudhi, A review of studies using nanofluids in flat-plate and direct absorption solar collectors, Renew. Sustain. Energy Rev. 84 (2018) 54–74.
[7] H. Duan, Analysis on the extinction properties of nanofluids for direct solar absorption, Physica E 120 (2020) 114046.
[8] Y.L. Hewakuruppu, R.A. Taylor, H. Tyagi, V. Khullar, T. Otanicar, S. Coulombe, N. Hordy, Limits of selectivity of direct volumetric solar absorption, Sol. Energy 114 (2015) 206–216.
[9] A.H. Elsheikh, S.W. Sharshir, M.E. Mostafa, F.A. Essa, M.K. Ahmed Ali, Applications of nanofluids in solar energy: A review of recent advances, Renew. Sustain. Energy Rev. 82 (2018) 3483–3502.
[10] X. Chen, P. Zhou, M. Chen, Enhancing the solar absorption performance of nanoparticle suspensions by tuning the scattering effect and incident light location, Int. J. Therm. Sci. 177 (2023) 107547.
[11] Y. Zou, L. Xiaoke, L. Yang, B. Zhang, X. Wu, Efficient direct absorption solar collector based on hollow TiN nanoparticles, Int. J. Therm. Sci. 185 (2023) 108099.
[12] M. Sheikholeslami, M. Jafaryar, Thermal assessment of solar concentrated system with utilizing CNT nanoparticles and complicated helical turbulator, Int. J. Therm. Sci. 184 (2023) 108015.
[13] S. Liang, F. Xu, H. Yang, S. Cheng, W. Yang, Z. Yi, Q. Song, P. Wu, J. Chen, C. Tang, Ultra long infrared metamaterial absorber with high absorption and broad band based on nano cross surrounding, Opt. Laser Technol. 158 (2023) 108789.
[14] F. Zhou, F. Qin, Z. Yi, W. Yao, Z. Liu, X. Wu, P. Wu, Ultra-wideband and wide-angle perfect solarenergy absorber based on Ti nanorings surfaceplasmon resonance, Phys. Chem. Chem. Phys. 23 (2021) 17041.
[15] F. Zhao, J. Lin, Z. Lei, Z. Yi, F. Qin, J. Zhang, L. Liu, X. Wu, W. Yang, P. Wu, Realization of 18.97% theoretical efficiency of 0.9 lm thick c-Si/ZnO heterojunctionultrathin-film solar cellsviasurface plasmonresonance enhancement, Phys. Chem. Chem. Phys. 24 (2022) 4871.
[16] S.U.S. Choi, J.A. Eastman, Enhancing thermal conductivity of fluids with nanoparticles, in: American Society of Mechanical Engineers, Fluids Engineering Division (Publication) FED, vol. 231, 1995, pp. 99–105.
[17] J. Hou, J. Du, H. Sui, L. Sun, A review on the application of nanofluids in enhanced oil recovery, Front. Chem. Sci. Eng. 16 (2022) 1165–1197.
[18] W. Yu, H. Xie, A review on nanofluids: Preparation, stability mechanisms, and applications, J. Nanomater. 2012 (2012) 435873.
[19] Z. Said, L.S. Sundar, A.K. Tiwari, H.M. Ali, M. Sheikholeslami, E. Bellos, H. Babar, Recent advances on the fundamental physical phenomena behind stability, dynamic motion, thermophysical properties, heat transport, applications, and challenges of nanofluids, Phys. Rep. 946 (2022) 1–94.
[20] R. Taylor, S. Coulombe, T. Otanicar, P. Phelan, A. Gunawan, W. Lv, G. Rosengarten, R. Prasher, H. Tyagi, Small particles, big impacts: A review of the diverse applications of nanofluids, J. Appl. Phys. 113 (1) (2013) 011301.
[21] A. Wahab, A. Hassan, M.A. Qasim, H.M. Ali, H. Babar, M.U. Sajid, Solar energy systems – Potential of nanofluids, J. Mol. Liq. 289 (2019) 111049.
[22] M. Turkyilmazoglu, Single phase nanofluids in fluid mechanics and their hydrodynamic linear stability analysis, Comput. Methods Programs Biomed. 187 (105171) (2020).
[23] M. Turkyilmazoglu, Nanoliquid film flow due to a moving substrate and heat transfer, Eur. Phys. J. Plus 135 (781) (2020).
[24] B.V. Balakin, P.G. Struchalin, Eco-friendly and low-cost nanofluid for direct absorption solar collectors, Mater. Lett. 330 (2023) 133323.
[25] M. Alberghini, M. Morciano, L. Bergamasco, M. Fasano, L. Lavagna, G. Humbert, E. Sani, M. Pavese, E. Chiavazzo, P. Asinari, Coffee-based colloids for direct solar absorption, Sci. Rep. 9 (2019) 4701.
[26] F.A. Essa, A.H. Elsheikh, A.A. Algazzar, R. Sathyamurthy, M.K. Ahmed Ali, M.A. Elaziz, K.H. Salman, Eco-friendly coffee-based colloid for performance augmentation of solar stills, Process Saf. Environ. Prot. 136 (2020) 259–267.
[27] A. Kosinska, B.V. Balakin, P. Kosinski, Use of biodegradable colloids and carbon black nanofluids for solar energy applications, AIP Adv. 11 (2021) 055214.
[28] S.P. Tembhare, D.P. Barai, B.A. Bhanvase, Performance evaluation of nanofluids in solar thermal and solar photovoltaic systems: A comprehensive review, Renew. Sustain. Energy Rev. 153 (2022) 111738.
[29] A. Kosinska, B.V. Balakin, P. Kosinski, Photothermal conversion of biodegradable fluids and carbon black nanofluids, Sci. Rep. 12 (2022) 3398.
[30] Z. Luo, C. Wang, W. Wei, G. Xiao, M. Ni, Performance improvement of a nanofluid solar collector based on direct absorption collection (DAC) concepts, Int. J. Heat Mass Transfer 75 (2014) 262–271.
[31] T.P. Otanicar, P.E. Phelan, R.S. Prasher, G. Rosengarten, R.A. Taylor, Nanofluid-based direct absorption solar collector, J. Renew. Sustain. Energy 2 (2010).
[32] A. Gimeno-Furio, L. Hernandez, N. Navarrete, R. Mondragon, Characterisation study of a thermal oil-based carbon black solar nanofluid, Renew. Energy 140 (2019) 493–500.
[33] E.T. Ulset, P. Kosinski, Y. Zabednova, O.V. Zhdaneev, P.G. Struchalin, B.V. Balakin, Photothermal boiling in aqueous nanofluids, Nano Energy 50 (2018) 339–346.
[34] E.T. Ulset, Utilizing Solar Vapour Energy By Use of Nanofluids in a Direct Absorption Solar Collector (Ph.D. thesis), University of Bergen, Norway, 2018.
[35] B. Ruan, A.M. Jacobi, Ultrasonication effects on thermal and rheological properties of carbon nanotube suspensions, Nanoscale Res. Lett. 7 (2012) 127.
[36] N. Goel, R.A. Taylor, T. Otanicar, A review of nanofluid-based direct absorption solar collectors: Design considerations and experiments with hybrid PV/Thermal and direct steam generation collectors, Renew. Energy 145 (2020) 903–913.
[37] P.G. Struchalin, V.S. Yunin, K.V. Kutsenko, O.V. Nikolaev, A.A. Vologzhannikova, M.P. Shevelyova, O.S. Gorbacheva, B.V. Balakin, Performance of a tubular direct absorption solar collector with a carbon-based nanofluid, Int. J. Heat Mass Transfer 179 (2021) 121717.
[38] V. Cregan, T.G. Myers, Modelling the efficiency of a nanofluid direct absorption solar collector, Int. J. Heat Mass Transfer 90 (2015) 505–514.
[39] R. Bårdsgård, D.M. Kuzmenkov, P. Kosinski, B.V. Balakin, Eulerian CFD model of direct absorption solar collector with nanofluid, J. Renew. Sustain. Energy 12 (3) (2020).
[40] J.J. Michael, I. S, R. Goic, Flat plate solar photovoltaic–thermal (PV/T) systems: A reference guide, Renew. Sustain. Energy Rev. 51 (2015) 62–88.
[41] M.A. Karim, O. Arthur, P.K. Yarlagadda, M. Islam, M. Mahiuddin, Performance investigation of high temperature application of molten solar salt nanofluid in a direct absorption solar collector, Molecules (2019) 1–27.